A hysteresis model for ferroelectric ceramics with mechanism for minor loops

Dan Wang [a,b], Linxiang Wang [a,*], Roderick Melnik [b]

[a] *State Key Laboratory of Fluid Power and Mechatronic Systems, Zhejiang University, 310027 Hangzhou, China*
[b] *MS2Discovery Interdisciplinary Research Institute, Wilfrid Laurier University, Waterloo, ON N2L 3L5, Canada*

ARTICLE INFO

ABSTRACT

In the current paper, the coupled hysteretic behaviors of ferroelectric ceramics subjected to combined electromechanical stimulations are modeled. For a single grain, the polarization orientation switching process is modeled by employing the Euler–Lagrange equations and formulated as a coupled differential equation system. For ferroelectric ceramics, the principle axis orientations of the individual grains are assumed to be distributed in a certain profile, the behaviors of the ceramics are modeled as a weighted combination of the response of each grain. The influence of intergranular interactions is carefully discussed. Numerical results for the minor hysteresis loops in strain and polarization are demonstrated. Comparisons between these results and their experimental counterparts are presented to illustrate the attributes of the proposed model.

© 2016 Elsevier B.V. All rights reserved.

1. Introduction

Due to their inherent electromechanical coupling properties, nowadays ferroelectric ceramics are widely used in many applications, including devices for vibration control and nano-positioners, camera focusing and shutter mechanisms, shape modification and flow control, and energy harvesting devices. However, when the ferroelectric ceramics are considered for device design and control applications, it is necessary to account that they typically operate in a nonlinear manner and hysteresis is present in the input–output relations. To take full advantages of the materials' properties, and to analyze, control, as well as optimize the ferroelectric devices, an efficient model which can capture the complex nonlinearities with coupled hysteretic effects is essential.

Currently, there are primarily two modeling strategies, which are based on the micromechanical models and the phenomenological models, respectively. The micromechanical models have been developed by energy characterization or thermodynamic description at the level of a single lattice cell, single domain, or single crystal. This strategy needs to be combined with various homogenization techniques (e.g., the Reuss approximations and different self-consistent averaging techniques) to provide the macroscopic input–output relations of the materials under investigation. Micromechanical models could accurately predict the responses of

the materials, but the numerical cost is very demanding since there are a large number of internal variables associated with the models. More details about micromechanical models could be found in Refs. [1–5] and references therein. Instead, the phenomenological models are based on the macroscopic experimental observations. Thermodynamic constrains play an important role in many phenomenological models to deduce the macroscopic relationships. A popular type of phenomenological models is the operator-based model, especially the Prandtl–Ishlinskii model, which is currently widely employed in the literature for its simplicity and analytical inversion [6–9]. Unlike the micromechanical models, the phenomenological models describe the input–output relations at a reduced calculation cost, but the high precision and generality is also compromised. Particularly, the phenomenological models have difficulties in capturing the coupled hysteresis loops accurately in the elastic and electric fields, as well as in modeling the rate dependence and stress dependence simultaneously.

In addressing the above mentioned challenges, the homogenized energy model, which was first proposed in Refs. [3,10] and then extended in Refs. [11–13,15] to account for the coupled electromechanical effects, is very attractive. This model can be thought as a micromechanical model in a sense that it handles the energy analysis at the domain level. A non-convex Helmholtz free energy is constructed to characterize different stable polarization orientations and the relation in the domain level is modeled by employing statistical mechanics. The volume fractions of different polarization orientations are selected as the internal variables. The macroscopic

* Corresponding author.
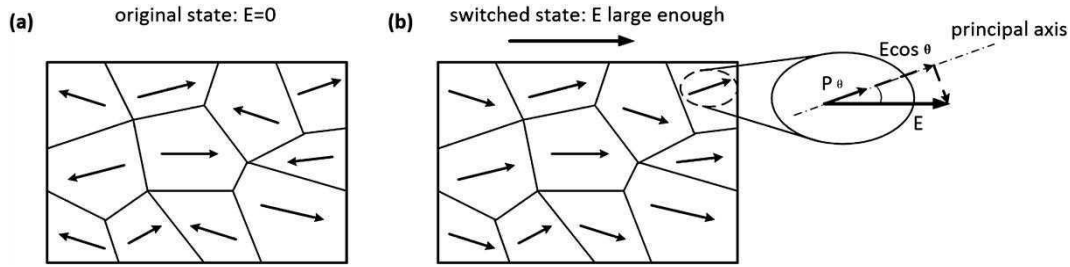*E-mail address:* wanglx236@zju.edu.cn (L. Wang).

Fig. 1. (a) A typical distribution of the principal axes in a poly-crystal ferroelectric material; (b) projection of the electric field to the principal axis of a grain.

model is obtained by assuming that the properties such as coercive fields, the interaction fields and critical driving forces are manifestation of underline densities rather than constants. We note that the associated parameter estimation and approximate inversion problems identified with this model are also well-studied [14,15,24,25]. The homogenized energy model can predict various phenomena in ferroelectric ceramics with high precision including the rate-dependent effects, creep effects and the stress-dependent effects. However, the numerical cost associated with the model can be demanding, especially for rate-dependent applications, due to the two-dimensional quadrature arising in the homogenization step of the model.

In the current paper, a phenomenological model is proposed based on the analysis and modeling of the polarization orientation switching in the materials, which is the origin of the hysteretic dynamics. In a single grain, the polarization orientation switching is formulated as a coupled differential system by employing the Euler–Lagrange equations. This allows us to model the electromechanical coupled phase transition. For such single crystal model, the internal variables are chosen based on the polarization and strain, and the volume fraction is not needed. For the modeling of ferroelectric ceramics, the contributions of all grains need to be taken into account. For the sake of simplicity, the detailed grain configuration is not considered. Instead, the principal axis orientations of individual grains in the materials are assumed distributed in a certain way, while the hysteretic dynamics associated with the electromechanical phase transition is regarded the same in all the grains along their principle axis orientation. Therefore, the overall dynamics of the ceramics along the field direction could be modeled as a weighted combination of the response in each grain. Furthermore, the intergranular interactions can be easily incorporated into the model. By taking this approach, the numerical expenses are dramatically reduced, while the accuracy of the model results is retained. In addition, the paper provides a detailed discussion about minor loops construction due to its vital importance in real applications. As for the inverse of current model, it will be discussed in our future paper for the length limit. However, it needs to be pointed out, considering the similarity between our model and the homogenized energy model, the progress in homogenized energy model will help us a lot.

2. Single-crystal model

It is well accepted nowadays that the physical essence of the unique behaviors of ferroelectrics lies in polarization orientation switching [1–5,16–21], therefore it is natural to construct a model by mimicking mathematically the process of polarization orientation switching. It was shown in Refs. [19,20] that, in one dimensional cases, the polarization orientation switching upon electromechanical loadings could be modeled by following the same strategy as for phenomenological theory of phase transitions. The governing equations for the switching dynamics could be obtained by employing the Euler–Lagrange equation as a coupled system of ordinary differential equations given as:

$$\tau_P \frac{dP}{dt} + a_2 P + a_4 P^3 + a_6 P^5 + 2b\varepsilon P - E = 0,$$
$$\tau_\varepsilon \frac{d\varepsilon}{dt} + k\varepsilon + bP^2 - \sigma = 0, \tag{1}$$

where τ_P and τ_ε are parameters related to the material properties. Note that the above governing equations is a simplified version based on the observation that the relaxation effects of polarization switching normally are much more pronounced than the inertial effects. Given the dominance of the relaxation effects of polarization switching, it has been confirmed that the coupled hysteretic dynamics of ferroelectric single crystals can be efficiently modeled by the above system of differential equations [19,20].

3. Polycrystalline model

For the modeling of ferroelectric ceramics, some extensions must be made to take into account the contributions of different grains. Assume that, the orientations of the principal axes of the grains in the ceramics are distributed in a certain profile, different from the uniform distribution, as sketched in Fig. 1(a). Let's consider a grain whose principal axis has an angle θ with respect to the direction of the applied electric field. The polarization orientation switching process along the principal axis thus is governed by the same dynamics as formulated in Eq. (1), which is re-written as the following:

$$\tau_P \frac{dP_\theta}{dt} + a_2 P_\theta + a_4 P_\theta^3 + a_6 P_\theta^5 + 2b\varepsilon P_\theta - E\cos\theta = 0,$$
$$\tau_\varepsilon \frac{d\varepsilon_\theta}{dt} + k\varepsilon_\theta + bP_\theta^2 - \sigma\cos\theta = 0, \tag{2}$$

where θ is the angle between the principal axis and the external field and $E\cos\theta$ and $\sigma\cos\theta$ are the projections of the external field and stress, respectively.

To clarify the effects of θ, a simulation with different θ values is presented in Fig. 2. The effects of the distributed principal axes are mainly represented by the distributed coercive fields. With a larger θ value, the component of field along the principal axis is smaller. Thus a stronger external electric field is needed to switch the polarization. The polarization and strain contributions of each grain to the overall response should be projected back to the external field direction. The whole polarization and strain under the stimulation of the external electric field and stress therefore are expressed as:

$$P = \int\limits_{all\,\theta} P_\theta w(\theta)\cos\theta \cdot d\theta = \int\limits_{all\,\theta} P_\theta \lambda(\theta) \cdot d\theta,$$
$$\varepsilon = \int\limits_{all\,\theta} \varepsilon_\theta w(\theta)\cos\theta \cdot d\theta = \int\limits_{all\,\theta} \varepsilon_\theta \lambda(\theta) \cdot d\theta, \tag{3}$$

where $w(\theta)$ represents the volume percentage of the grains whose principal axes have a θ angle with respect to the external field and $\lambda(\theta)$ is a weight function which includes the influence of $\cos(\theta)$.
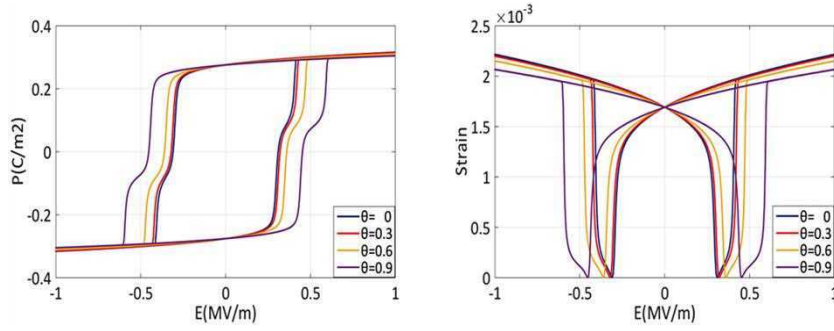
Fig. 2. Effects of the θ value on the responses of the grains in the material: (a) field-polarization curves, (b) field–strain curves.

Thus, Eq. (2) and Eq. (3) together constitute the governing equations for the macroscopic level of modeling of the ferroelectric ceramics.

The proposed model given by Eq. (2) and Eq. (3) is easily understood. However, as shown in Fig. 2, the evenly-distributed θ value leads to a non-evenly-distributed coercive field, which implies disadvantages in the numerical calculation. Therefore, a simple transformation is made by dividing both sides of the equations in Eq. (2) by $\cos\theta$, and the dynamic model is written as the following:

$$T_P \frac{dP_c}{dt} + A_2 P_c + A_4 P_c^3 + A_6 P_c^5 + 2B\varepsilon P_c - E = 0,$$

$$T_\varepsilon \frac{d\varepsilon_c}{dt} + K\varepsilon_c + BP_c^2 - \sigma = 0, \tag{4}$$

where $T_P = c \cdot \tau_P$, $A_2 = c \cdot a_2$, $A_4 = c \cdot a_4$, $A_6 = c \cdot a_6$, $T_\varepsilon = c \cdot \tau_\varepsilon$, $B = c \cdot b$, $K = c \cdot k$ with $c = 1/\cos\theta$. Now these seven parameters are distributed based on the factor c. Accordingly, P_θ is replaced by P_c and ε_θ by ε_c. It is easy to see that the coercive field is evenly-distributed when the factor c has an even distribution after the modification. Eq. (3) is changed in accordance with:

$$P = \int\limits_{all\,c} P_c \lambda(c) \cdot dc,$$

$$\varepsilon = \int\limits_{all\,c} \varepsilon_c \lambda(c) \cdot dc. \tag{5}$$

Clearly, the influence of the intergranular interactions was omitted in the derivation of the above governing equations. Considering its vital importance, the influence needs to be carefully discussed. And it will be shown that the effect of the intergranular interactions can be easily incorporated into the proposed model by modifying the weight function. Here, only the electric field interactions are dealt with for simplicity and similar strategies can be adapted to the elastic field interactions. When an external field E_{ex} is imposed, it is reasonable to treat the influence of the intergranular interactions on a specific grain as an additive field E_{add}. The additive field can be parallel or antiparallel to the external field, which depends on the current polarization state. The current polarization state is history-dependent. Thus, the polarization orientation switching process in the specific grain can take place ahead of time or behind, which means the effective coercive field in the grain is changed. At macroscopic level, the profile of the weight function should be altered in accordance.

To clearly interpret the influence of the intergranular interactions, three typical states in a hysteresis loop are illustrated in Fig. 3. When the external electric field is increased from the negative saturation region to point A, most of the polarizations have not been switched. For a specific grain as shown in the figure, apart from the external field E_{ex}, the polarizations of other grains will impose an additive field E_{add} on it. Here the additive field
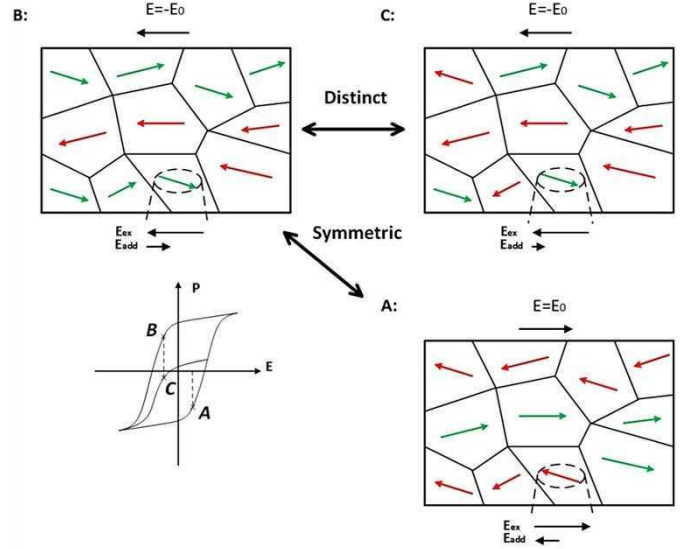

Fig. 3. Illustration of the influence of intergranular interactions on a specific grain for three different polarization configurations.

is antiparallel to the external field since most of the polarizations have not been switched at this point. The antiparallel additive field will cause a delayed polarization switching of the specific grain, which means a larger effective coercive field in the grain and a changed profile of the weight function at macroscopic level. When the external electric field is decreased from the positive saturation region to point B (where the external field is opposite to the electric field of point A), most of the polarizations have not been switched back. The configuration of the polarization is similar to that of point A but has an opposite direction, as shown in the figure. So the additive field for the specific grain has the same length but opposite direction to the additive field at point A. Considering the symmetry, it can be concluded that the effective weight function corresponding to the major loop either for the ascend branch or the descend branch will have the same profile. However, as shown in the figure, when the external field decreased from a non-saturation region to point C, the configuration of the polarization is distinct from that of point B. Thus the additive field for the specific grain will be different, which means a different weight function profile. So the weight function regarding the minor loops will be different from that of the major loops and this can be considered as the physical origin of 'redistribution of the weight function' in minor loops construction. This mechanism will be carefully discussed in the following sections. In conclusion, the weight function in the provided model is comprised of two parts—an intrinsic weight function which corresponds to the weight of the principal axes, and a modified weight function which takes the influence of the intergranular interactions into account. But

the two different parts are treated indiscriminatingly in numerical simulation.

4. The weight function

The new factor c introduced in Eq. (4) and Eq. (5) plays a role similar to a scaling factor of the coercive field. When c equals 1, the coercive field will take the value such that the external field is applied along the principal axis of the single-crystal. Theoretically $c \geq 1$ and a larger factor c means a larger coercive field. As pointed out above, the value of factor c is distributed in a certain profile which could be specified by a weight function. The weight function plays a key role in the proposed model, and some requirement should be fulfilled:

(i) $\lambda(c)$ is defined for $c \geq 1$,
(ii) $|\lambda(c)| \leq m \cdot e^{-n \cdot c}$, where m and n are some positive numbers.

Condition (i) reflects the mathematical fact that $1/\cos\theta$ can never be smaller than 1 for all θ values, while requirement (ii) reflects the assumption that the volume ratio of the grain having a principle axis orientation along θ decreases as θ becomes larger. This requirement guarantees that the integration against the single-crystal loop yields finite polarization and strain values. A general phenomenological weight function could be obtained by fitting the model with the experimental data, as in Ref. [11]. The general weight function has a high degree of freedom and precision but it is inconvenient when conducting the parameter estimation. A simple explicit function can be constructed to approximate it. An obvious choice could be a log-normal density function, as proposed in the homogenized energy model, namely

$$\lambda(c) = \alpha e^{-[\ln(c/\bar{c})/\beta]^2} \tag{6}$$

where α, β and $\bar{c}$ are model parameters which need to be determined.

5. Minor loops construction

In simulating the hysteretic dynamics of ferroelectrics ceramics, the input signal can be asymmetric and non-periodic, and minor hysteresis loops occur. In order to fit the proposed model with experimental minor hysteresis loops, some modifications need to be incorporated. Since the first and second order reversal curves play a fundamental role in the minor loop construction process, it is carefully discussed as an illustration and the idea introduced here can be easily generalized to the case of higher order reversal curves. For simplicity, no rate-dependence property is taken into account here. When an electric field stimulation is applied from the negative saturation region, the polarization will increase reversely at first and the polarization orientation switching will take place after the field exceeds the minimum coercive field. To generate a first order reversal curve, the field will not be continuously increased to the positive saturation region and instead it is reversed at an unsaturation region like at field E_0. When the field is reversed at E_0, the switched polarization orientation will not switch back instantaneously. Like before, the polarization decreases reversely at first and the polarization orientation switching is induced when the field reaches the negative minimum coercive field. However, as in Fig. 4(a), the switched polarization orientations are all switched back at field $-E_0$ which means that point F coincides with point B which is not the case in real materials. To address this drawback, we assume that the weight function corresponding to the switched part will be redistributed along the whole range when the external field is reversed. The physical origin of the redistribution has been discussed above. It is well-known that there
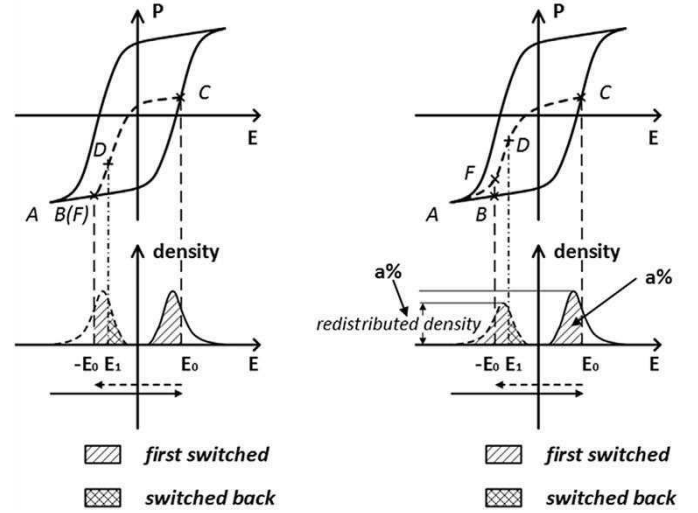

Fig. 4. Illustrations of the construction of the first order reversal curve: (a) original model; (b) model with a redistributed weight function.
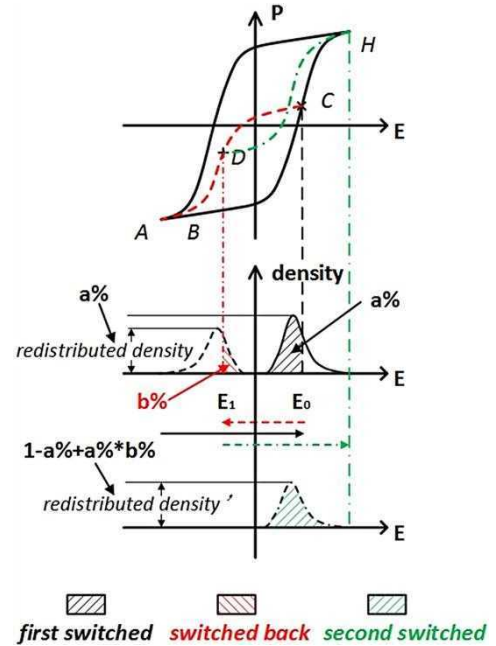

Fig. 5. Illustrations of the construction of the first order reversal curve.

are some similarities between the first order reversal curves and the major loop, so the weight function pertinent to the switched part can be generated by taking a similar transformation of that with respect to the major loop. Here, we'll scale the major loop's weight function directly for simplicity and the scaling factor equals the portion of the first switched part to the whole grains (which is $a\%$ in Fig. 4(b)). Thus, the first switched part cannot all be switched back until the field reaches the negative saturation region which results in the distinct F and B points as in Fig. 4(b). The first order reversal curves generated in such a way seem better suitable for applications.

In addition, construction of the second reversal curves is illustrated in Fig. 5. A second reversal curve is generated, when the external field, which has first been reversed at E_0 and has not reached the negative saturation region, is reversed again (at field E_1). Like before, the weight function needs to be redistributed. And the same strategy is taken here and the scaling factor in this case equals $1 - a\% + a\% * b\%$, where $1 - a\%$ represents the

portion that was not switched in the first stage (the stage before the external field was first reversed), $a\% * b\%$ represents the portion that was switched back in the second stage (the stage between the field's first and second reversions) and the sum means the whole portion that needs to be switched in this stage. The second reversal curves constructed in this way will tend to the saturation point H in a trajectory similar to the major loop, as shown in Fig. 5. In contrast, if the weight function is not redistributed, the second reversal curves will meet the major loop at point C and goes along the major loop beyond point C, which means that the famous 'wiping out' property will take place. Typically, 'wiping out' is a property that only occurs in static or quasi-static regimes and will not be true in rate-dependent regimes. From the physical view point, the behavior corresponding to the described weight function redistribution is more suitable for applications.

As shown in Fig. 5, a minor loop or inner loop will be presented when the second reversal curve meets the first reversal curve. As pointed above, the idea and strategy introduced here can be easily generalized to the case of higher order reversal curves.

6. Model validation and discussions

In the previous section we constructed a new phenomenological model based on polarization orientation switching. In this section, the proposed model will be numerically implemented and compared with experimental data to illustrate the main advantages and limitations of the model. The experimental data reported in Ref. [22] will be used for this purpose. A series of asymmetric electric fields were applied to a commercial soft-type PZT ceramics, and the polarization and strain hysteresis loops were measured simultaneously. The biased stress of the experiment was -4.5 MPa and the applied electric field was at a frequency of 0.25 Hz. For more details about the experimental conditions, the interested reader should consult Ref. [22]. There are 10 parameters that need to be estimated, τ_P, a_2, a_4, a_6, τ_ε, b and k in the single-crystal model and α, β and $\bar{c}$ in the weight function. Since the experimental data have been obtained at a fixed low frequency and frequency-dependent property is not considered here, frequency-related parameters τ_P and τ_ε are set to be fixed small values (here, $\tau_P = 0.003$, $\tau_\varepsilon = 0$). As we know, the sixth order polynomial, which is represented as a fifth order polynomial in the governing equations, will induce numerical instabilities. Hence, the piecewise cubic Hermit polynomials are used instead, and we will replace the fifth order polynomial in the governing equations directly. The parameters a_2, a_4 and a_6 thus are substituted by the interpolation points coordinates. As we can see, the parameter estimation problem involved here is strongly nonlinear and needs to be carefully studied. The parameter estimation in this paper is formed as a nonlinear least square optimization problem that can be written as follows:

$$\min_{model\ parameters} G = \sum_{i=1}^{M}\left(\left(\frac{\overline{P_i} - P_i}{P_{magnitude}}\right)^2 + \left(\frac{\overline{\varepsilon_i} - \varepsilon_i}{\varepsilon_{magnitude}}\right)^2\right), \quad (7)$$

where M is the number of experimental data samples, $\overline{P_i}$ and $\overline{\varepsilon_i}$ are experimental values of P and ε, P_i and ε_i are the corresponding simulated values, and $P_{magnitude}$ and $\varepsilon_{magnitude}$ are the magnitudes of the experimental data which are used to get the relative errors. It should be pointed out that the optimization problem formed here is a multi-objective one with respect to model parameters in order to obtain good agreement in both electric and mechanical fields. To achieve this, the relative errors are employed. Furthermore, a set of reasonable initial parameters are needed since that the nonlinear optimization problem is very sensitive to the initial parameters.
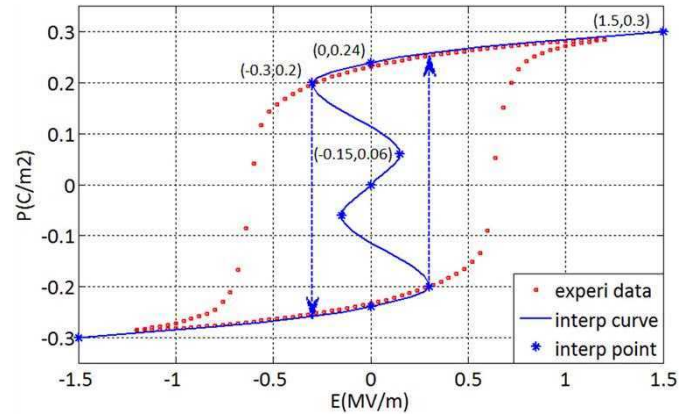

Fig. 6. Determination of the initial interpolation points coordinates for parameter estimation.

6.1. Initial parameter setting procedure

Firstly, the single-crystal model without the weight function is compared with the experimental data to give the initial estimation of the parameters—b, k and the interpolation points coordinates. The parameters b and k can be easily estimated from the P^2–ε relationships by formulating a linear least square problem, for by setting $\tau_\varepsilon = 0$, the second equation in the single-crystal model Eq. (1) is reduced to:

$$\varepsilon = -\frac{b}{k}P^2 + \frac{1}{k}\sigma, \quad (8)$$

where ε is a linear function of P^2. The obtained values of b and k are respectively -87.2 and 2360. Then the interpolation points coordinates are provided as $(1.5, 0.3)$, $(0, 0.24)$, $(-0.3, 0.2)$, $(-0.15, 0.06)$ by comparing the E–P curve in the constitutive equation with the experimental E–P curve, as shown in Fig. 6 [23]. As the curve is symmetric about the origin, only the interpolation points whose vertical coordinates are larger than 0 are given and all the vertical coordinates will be kept unchanged during parameter optimization.

The parameters related to the weight function are relatively easy to set as they will not usually induce numerical instabilities in the simulation. A set of reasonable values that have been used in this simulation are: $\alpha = 0.03$, $\beta = 0.4$ and $\bar{c} = 2.00$.

6.2. Results and discussions

With the initial parameter values given above, the nonlinear optimization problem is implemented in Matlab, where the simplex search method is applied. Clearly, there is no need to solve tens or hundreds nonlinear ordinary equations simultaneously when implementing the model, for there are some similarities between the responses of different principal axes and an affine transformation can be used. As a result, only one equation needs to be solved and other responses can be provided by the transformation. The calculation cost is largely reduced. The final estimated parameters are listed in Table 1 combined with the corresponding initial values. The comparisons between the simulated and experimental results are presented in Fig. 7. The major loop and minor loops are generally well-captured by the proposed model. As mentioned, only the electrostrictive effect (represented by the term εP^2) is considered for simplicity. If additional coupling effects are taken into consideration, the results will even be better. The results can also be improved with a general weight function.

Table 1
The initial and optimized value of the model parameters.

Parameter	Initial value	Optimized value
k	−87.2	−88.07
b	2.36e3	3.20e3
α	0.03	0.033
β	0.4	0.21
$\bar{c}$	2.00	1.79
Interpolation points coordinates[a]	(**1.5**, 0.3), (**0**, 0.24), (−**0.3**, 0.2), (**0.15**, 0.06)	(**1.5**, 0.33), (**0**, 0.1980), (−**0.3**, 0.1228), (**0.15**, 0.06)

[a] As pointed out above, the curves are symmetric about the origin, so only four interpolation coordinates are needed and the **E** coordinates are kept unchanged during the optimization procedure.
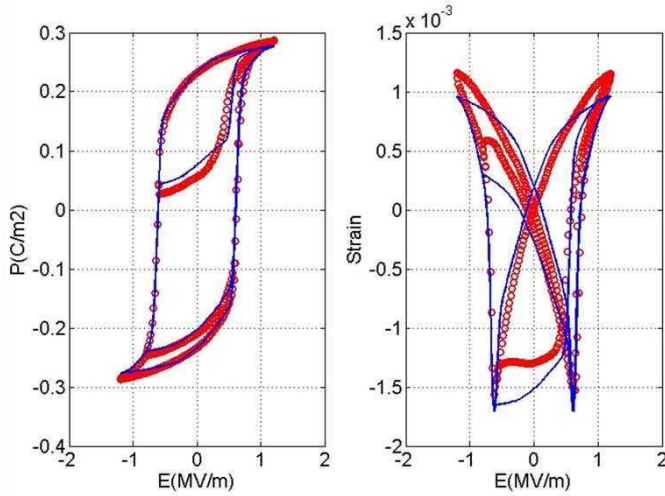

Fig. 7. Comparisons between the model predictions and experimental results. (Blue lines represent model predictions while the red circles represent experimental results.) (For interpretation of the references to color in this figure legend, the reader is referred to the web version of this article.)

Table 2
Model parameters for rate-dependent minor loop hysteresis.

Parameter	Estimated value
k/b[a]	−0.0267
α	0.0131
β	0.4038
$\bar{c}$	1.8987
τ_P	0.0027
Interpolation points coordinates	(**1.5**, 0.2645), (**0**, 0.2103), (−**0.3**, 0.1931), (**0.15**, 0.05)

[a] In this experiment/simulation, no bias stress is imposed, so the parameters k and b will merge into one single parameter.

6.3. Rate-dependent minor loop capability

To further demonstrate the model's capability for rate-dependent minor loop hysteresis, the experimental results presented in Ref. [26] are adopted. Series asymmetric electric field inputs with same loading path but different loading rates were fed into a ferroelectric actuator (Model P-802.00). The experiment was carried out under no bias stress. For more detailed information regarding the experimental condition, Ref. [26] can be referred to. Firstly, hysteresis loops with driving rates at 0.05 MV/m/sec and 5 MV/m/sec are used for parameter-estimation purpose. The estimated parameters are listed in Table 2. The comparisons of the current model simulations with their experimental counterparts are presented in Fig. 8(a) and Fig. 8(c). Then the estimated parameters are used for prediction for the experiment with driving rate
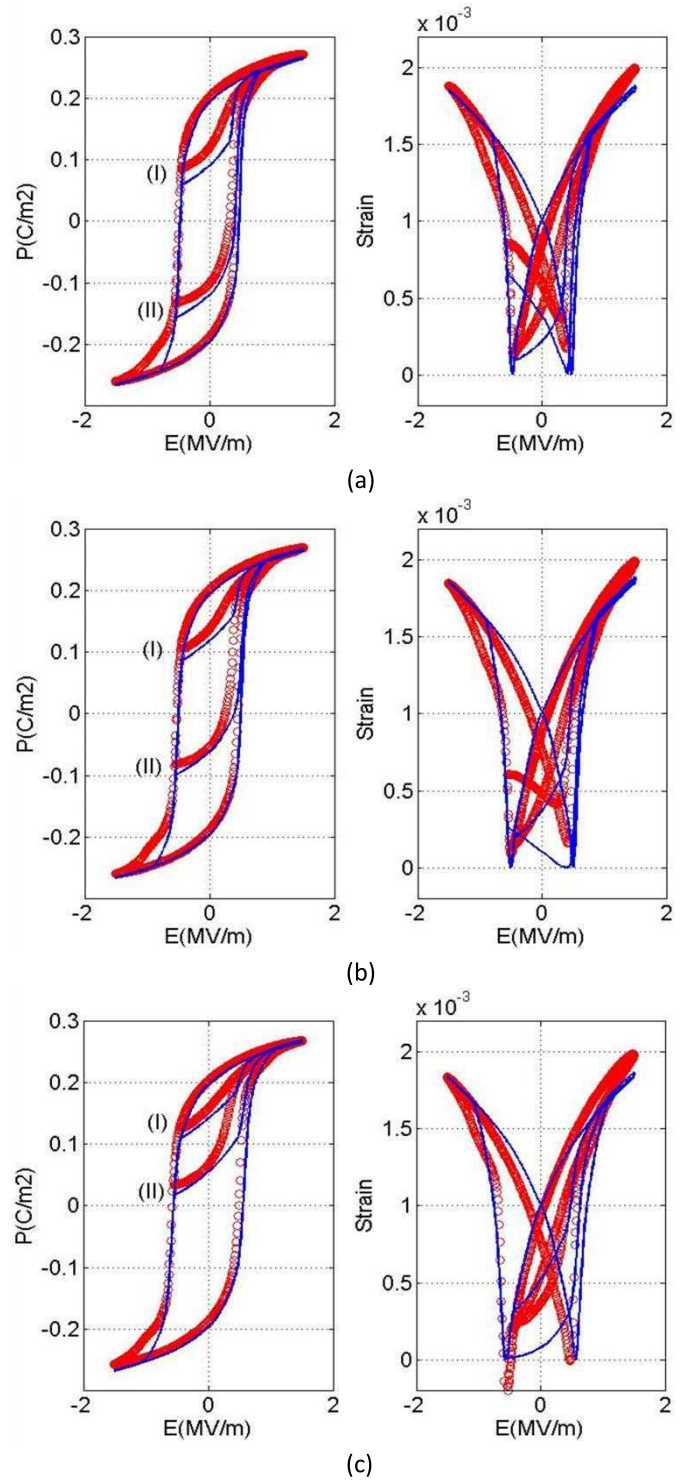

Fig. 8. Demonstration of rate-dependent minor loop hysteresis capability of the proposed model: (a) 0.05 MV/m/sec; (b) 0.5 MV/m/sec; (c) 5 MV/m/sec.

at 0.5 MV/m/sec and the results are shown in Fig. 8(b). Generally, the model can capture the rate-dependent minor loop hysteresis very well. With a higher driving rate, the hysteresis loop get fatter due to a delayed polarization switching process. Furthermore, the reversal points corresponding to same electric input value shift upwards as the driving rate increases. All these important features are well-captured by the proposed model as shown in the figure. As for another important rate-dependent phenomenon: creeping, it will be carefully discussed in our future papers.

D. Wang et al. / Physics Letters A 381 (2017) 344–350

7. Conclusions

In the current paper, a new phenomenological model for the coupled hysteretic behaviors in ferroelectrics ceramics has been presented. At the grain level, the microscopic governing equations have been obtained as a coupled system of differential equations by applying the Euler–Lagrange model. The principal axes of different grains in ferroelectric ceramics have been assumed to be distributed according to a pre-defined profile. As a result, the macroscopic models have been derived as a weighted combination of responses of each grain. The effect of intergranular interactions is naturally incorporated into the model through the weight function. Comparisons between the model predictions and experimental results have been presented, demonstrating that the major loop and minor loops are well-captured by the provided model. The model efficiency has been largely improved at the mathematical level, which means that the current model can lead to more efficient numerical implementations particularly important for model-based control theory and applications.

Acknowledgements

References

[1] C.M. Landis, Non-linear constitutive modeling of ferroelectrics, Curr. Opin. Solid State Mater. Sci. 8 (1) (2004) 59–69.
[2] J.E. Huber, Micromechanical modelling of ferroelectrics, Curr. Opin. Solid State Mater. Sci. 9 (3) (2005) 100–106.
[3] R.C. Smith, Smart Material Systems: Model Development (vol. 32), SIAM, 2005.
[4] K. Jayabal, A. Menzel, A. Arockiarajan, S.M. Srinivasan, Micromechanical modelling of switching phenomena in polycrystalline piezoceramics: application of a polygonal finite element approach, Comput. Mech. 48 (4) (2011) 421–435.
[5] S. Lange, A. Ricoeur, A condensed microelectromechanical approach for modeling tetragonal ferroelectrics, Int. J. Solids Struct. 54 (2015) 100–110.
[6] M. Al Janaideh, P. Krejci, Inverse rate-dependent Prandtl–Ishlinskii model for feedforward compensation of hysteresis in a piezomicropositioning actuator, IEEE/ASME Trans. Mechatron. 18 (5) (2013) 1498–1507.
[7] G.Y. Gu, L.M. Zhu, C.Y. Su, Modeling and compensation of asymmetric hysteresis nonlinearity for piezoceramic actuators with a modified Prandtl–Ishlinskii model, IEEE Trans. Ind. Electron. 61 (3) (2014) 1583–1595.
[8] M.J. Yang, C.X. Li, G.Y. Gu, L.M. Zhu, Modeling and compensating the dynamic hysteresis of piezoelectric actuators via a modified rate-dependent Prandtl–Ishlinskii model, Smart Mater. Struct. 24 (12) (2015) 125006.
[9] G.Y. Gu, L.M. Zhu, C.Y. Su, H. Ding, Modeling of piezoelectric-actuated nanopositioning stages involving with the hysteresis, in: Nanopositioning Technologies, Springer International Publishing, 2016, pp. 183–212.
[10] R.C. Smith, S. Seelecke, Z. Ounaies, J. Smith, A free energy model for hysteresis in ferroelectric materials, J. Intell. Mater. Syst. Struct. 14 (11) (2003) 719–739.
[11] B.L. Ball, R.C. Smith, S.J. Kim, S. Seelecke, A stress-dependent hysteresis model for ferroelectric materials, J. Intell. Mater. Syst. Struct. 18 (1) (2007) 69–88.
[12] A. York, Experimental characterization and modeling of electro-mechanically coupled ferroelectric actuators, ProQuest, 2008.
[13] R.C. Smith, Z. Hu, Homogenized energy model for characterizing polarization and strains in hysteretic ferroelectric materials: material properties and uniaxial model development, J. Intell. Mater. Syst. Struct. 23 (16) (2012) 1833–1867.
[14] R.C. Smith, A.G. Hatch, Parameter estimation techniques for a class of nonlinear hysteresis models, Inverse Probl. 21 (4) (2005) 1363.
[15] Z. Hu, R.C. Smith, J. Ernstberger, The homogenized energy model for characterizing polarization and strains in hysteretic ferroelectric materials: implementation algorithms and data-driven parameter estimation techniques, J. Intell. Mater. Syst. Struct. 23 (16) (2012) 1869–1894.
[16] C.S. Lynch, The effect of uniaxial stress on the electro-mechanical response of 8/65/35 PLZT, Acta Mater. 44 (10) (1996) 4137–4148.
[17] H. Sahota, Simulation of butterfly loops in ferroelectric materials, Contin. Mech. Thermodyn. 16 (1–2) (2004) 163–175.
[18] L.X. Wang, M. Willatzen, Extension of the Landau theory for hysteretic electric dynamics in ferroelectric ceramics, J. Electroceram. 24 (1) (2010) 51–57.
[19] L. Wang, R.V. Melnik, Control of coupled hysteretic dynamics of ferroelectric materials with a Landau-type differential model and feedback linearization, Smart Mater. Struct. 18 (7) (2009) 074011.
[20] L. Wang, Hysteretic dynamics of ferroelectric materials under electromechanical loadings, in: ASME 2008 Conference on Smart Materials, Adaptive Structures and Intelligent Systems, American Society of Mechanical Engineers, 2008, pp. 189–195.
[21] D. Zhou, M. Kamlah, D. Munz, Rate dependence of soft PZT ceramics under electric field loading, in: Smart Structures & Materials Active Materials Behavior & Mechanics, in: Proc. SPIE, vol. 4333, 2001, pp. 64–70.
[22] Y. Kadota, H. Hosaka, T. Morita, Field-induced strain memory with non-180 domain-reorientation control, J. Korean Phys. Soc. 57 (4) (2010) 902–906.
[23] L.X. Wang, M. Willatzen, Nonlinear dynamical model for hysteresis based on nonconvex potential energy, J. Eng. Mech. 133 (5) (2007) 506–513.
[24] T.R. Braun, R.C. Smith, Efficient inverse compensation for hysteresis via homogenized energy models, in: The 14th International Symposium on: Smart Structures and Materials & Nondestructive Evaluation and Health Monitoring, International Society for Optics and Photonics, 2007, p. 65261A.
[25] J.A. McMahan, J.H. Crews, R.C. Smith, Inversion algorithms for the homogenized energy model for hysteresis in ferroelectric and shape memory alloy compounds, J. Intell. Mater. Syst. Struct. 24 (15) (2013) 1796–1821, http://dx.doi.org/10.1177/1045389X12471868.
[26] A. York, Experimental characterization and modeling of electro-mechanically coupled ferroelectric actuators, ProQuest, 2008.